Published in final edited form as:
IEEE Trans Geosci Remote Sens. 2016 February ; 54(2): 1103–1117. doi:10.1109/TGRS.2015.2474120.

Calibration to improve forward model simulation of microwave emissivity at GPM frequencies over the U.S. Southern Great Plains

Kenneth W. Harrison[1,2], **Yudong Tian**[1,2], **Christa D. Peters-Lidard**[2], **Sarah Ringerud**[3], and **Sujay V. Kumar**[2,4]

[1]Earth System Science Interdisciplinary Center, University of Maryland, College Park, MD

[2]Hydrological Sciences Laboratory, NASA, Goddard Space Flight Center, Greenbelt, MD

[3]Colorado State University, Fort Collins, Colorado, USA

[4]Science Applications International Corporation, Beltsville, MD

Abstract

Better estimation of land surface microwave emissivity promises to improve over-land precipitation retrievals in the GPM era. Forward models of land microwave emissivity are available but have suffered from poor parameter specification and limited testing. Here, forward models are calibrated and the accompanying change in predictive power is evaluated. With inputs (e.g., soil moisture) from the Noah land surface model and applying MODIS LAI data, two microwave emissivity models are tested, the Community Radiative Transfer Model (CRTM) and Community Microwave Emission Model (CMEM). The calibration is conducted with the NASA Land Information System (LIS) parameter estimation subsystem using AMSR-E based emissivity retrievals for the calibration dataset. The extent of agreement between the modeled and retrieved estimates is evaluated using the AMSR-E retrievals for a separate 7-year validation period. Results indicate that calibration can significantly improve the agreement, simulating emissivity with an across-channel average root-mean-square-difference (RMSD) of about 0.013, or about 20% lower than if relying on daily estimates based on climatology. The results also indicate that calibration of the microwave emissivity model alone, as was done in prior studies, results in as much as 12% higher across-channel average RMSD, as compared to joint calibration of the land surface and microwave emissivity models. It remains as future work to assess the extent to which the improvements in emissivity estimation translate into improvements in precipitation retrieval accuracy.

Keywords

Remote sensing; Radiometry; Parameter estimation

Corresponding author: Ken Harrison, Hydrological Sciences Laboratory (Code 617), NASA Goddard Space Flight Center (GSFC), 8800 Greenbelt Rd., Greenbelt, MD 20771, Tel: (301) 286-7095; Fax: (301) 614-5808, ken.harrison@nasa.gov.

Introduction

Better characterization of the dynamics of land surface microwave emissivity (MWE) holds promise for improving precipitation retrievals in the Global Precipitation Measurement (GPM) era [1], in which coverage extends to higher latitudes (68°). This study concerns the forward model simulation of MWE, which consists of the coupling of a land surface model (LSM), forced by meteorological data, to a microwave emissivity model (MEM). The work presented builds off of the study of Ringerud et al. [2] that assessed the potential of forward model simulation of MWE for GPM. The study is distinguished from Ringerud et al. [2] in that here the parameters of the forward models are tuned to improve predictive power. We compare calibrated forward models against un-calibrated forward models in their ability to simulate MWE, using MWE retrievals as a benchmark. Here, the analysis is limited to MWE, leaving evaluation of the impact to precipitation retrievals to future work.

The land surface microwave emission is important as it obscures the signal of the precipitation retrieval [3]. MWE can vary widely given its sensitivity to soil moisture and vegetation. Bare soil MWE responds to soil moisture changes due to the large dielectric constant of water, with MWE decreasing with increasing soil moisture. Vegetative cover absorbs and scatters the underlying soil MWE signal, and very dense vegetation can completely obscure the soil MWE signal. If very dense, the signal is that of the vegetation, which is very high.

Like Ringerud et al. [2], we focus on the MWE dynamics in the U.S. Southern Great Plains (SGP; 34°N:39°N, 100°W:95°W) as the SGP exhibits a large MWE variation, both spatially and temporally, attributable to the pronounced soil moisture and vegetation dynamics. The SGP is characterized by abundant cropland but also has representation of other land covers, and a range of soils classes. Unlike Ringerud et al. [2], we restrict the focus of the study to the MWE simulation of the soil-vegetation system as snow, frozen ground, and distinct land types (e.g., deserts, wetlands), which also strongly impact MWE, present distinctly different modeling challenges.

For the GPM radiometer precipitation retrievals, forward models can supply the MWE estimates that are required for full forward model simulation of top-of-atmosphere brightness temperatures, which is needed for construction of the physical database. This database, which is searchable by the retrieval algorithm, relates a set of geophysical parameters with brightness temperatures at all relevant frequencies and polarizations [4–6]. Forward modeling also can provide a supporting role by helping to determine a sufficient set of emissivity-related globally available geophysical quantities (e.g., LAI, soil moisture, surface temperature, total precipitable water (TPW) by which to index into the precipitation retrieval database. Current work is ongoing assessing the level of accuracy required for these fields at the algorithm level. Alternatives to forward modeling address MWE more indirectly, and include the identification of “surface-blind” pseudo-channels [7, 8], indexing by similarity classes based on monthly MWE climatology [9], empirical approaches to account for recent precipitation [10, 11], and hybrid approaches that combine both modeling and statistical approaches [12, 13]. As it underpins the similarity class [9] method, a climatological approach to MWE estimation is also evaluated (in which daily estimates are

interpolated from monthly means). This provides a point of reference for assessing the value of capturing MWE dynamics with forward models.

The forward model configuration is similar to Ringerud et al. [2], consisting of the Noah LSM (v.3.3) coupled to the land MEM of the Community Radiative Transfer Model (CRTM) developed by the Joint Center for Satellite Data Assimilation (JCSDA). Here, we also test a coupling of Noah to the Community Microwave Emission Model (CMEM) developed by the European Centre for Medium-Range Weather Forecasts (ECMWF). Both MEMs are used in globally run operational satellite data assimilation systems. We use as a benchmark the same set of cloud-cleared MWE retrievals developed by Ringerud et al. [2] but, with our focus here on the soil-vegetation system, clearing for snow and frozen-ground conditions, and reserving a portion, a single warm season (2008 April-September), for calibration.

The first motivating factor for calibration is the finding of large simulation errors of forward models and their LSM and MEM constituents. In LSM inter-comparison studies focused on soil moisture, including in the SGP area [14], while LSMs have been shown to have some skill in simulating anomalies, large root-mean-square-errors and biases are reported. The story is similar for MEMs. Weng et al. [15], who ran CRTM over bare soil and short grass at five microwave frequencies (4.9–94 GHz), while noting agreement in broad features, including MWE spectra, variability, and polarization, reported sizeable biases. Uncertainty propagation and sensitivity studies involving CMEM have also indicated large forward modeling MWE simulation errors [16, 17]. Ringerud et al. [2], also finding large errors, concluded that forward models were not yet suitable for precipitation retrievals. The GPM passive microwave algorithm team has estimated that an accuracy of 1% or better is required for the coupling of emissivity to the physical atmosphere retrieval, and separation of dynamic surface emission from emission by hydrometeors in the atmosphere [2]. An accuracy of 3% emissivity, while sufficient for retrievals of heavy rain, would be insufficient for discriminating rain/no rain events and retrievals of lighter precipitation [3].

The second motivating factor for calibration is the poor specification of LSM and MEM parameters, which likely contributes a great amount of error. On the LSM side, many parameters are specified via tables indexed by variables such as soil texture and land cover. The limitations of lookup tables are well documented for soil moisture modeling [18, 19], and relate to the representativeness of the underlying soils databases [19–21] and the accuracy of the inputs (i.e., soil texture maps) themselves [22]. On the MEM side, parameters similarly are poorly specified. Weng et al. [15] attributed much of the bias in CRTM predictions to the “arbitrary” specification of many important parameters, including land surface roughness, leaf thickness, and canopy gravimetric water content, due to the lack of available data.

Given the poor specification of both LSM and MEM parameters, here we jointly calibrate the LSM and MEM. This is a significant departure from prior related studies calibrating to remote sensing data. In one set of studies [18, 21, 23–26], LSMs are calibrated to remote sensing data products (e.g., soil moisture, soil temperature), the generation of which relies on radiative transfer modeling that itself suffers from parameter misspecification. In the

other batch of studies [27–30], MEMs were calibrated to brightness temperature data products, taking inputs from un-calibrated LSMs. (In some cases, the LSM was not simultaneously calibrated as this would upset model climatology [28, 29].) The approach of jointly estimating the LSM and MEM is further motivated by prior studies specifically attributing errors in forward modeled MWE to errors in soil moisture dynamic range [27, 30]. Given this departure from previous studies, we compare also the benefits, if any, of joint calibration over the independent calibration of the LSM or MEM.

The forward modeling is conducted using NASA Goddard Space Flight Center's (GSFC) Land Information System (LIS), with the calibration done using the LIS optimization and uncertainty estimation subsystem (LIS OPT/UE) [31, 32]. As in several recent studies [28–30], the MEM parameters are "locally" estimated, i.e., optimal parameter sets are sought for each grid cell, and a stochastic search algorithm is applied. This approach is distinct from other studies (e.g., [27]) in which an ad-hoc search was applied to identify a single best "global" parameter set.

The focus here is on assessing calibration's impact on the forward models' predictive ability, and not on evaluation of the physical consistency of the resultant parameter values. The hydrological literature is replete with examples, even in field or finer-scale studies [18, 23, 33–35], of calibration of more physically complete models leading to significant and important improvements in simulation but resulting in parameter values inconsistent with *in situ* measurement. There are several theoretical reasons for this seeming dissonance, including parameter distortions introduced from the necessary model simplifications [36], the incompleteness of the error models employed [36–40], and inability to access and tune hard-coded parameters [41], and an active area of research exists exploring these issues [18, 40, 42–49]. An additional problem is the lack of *in situ* data of a spatial sampling density sufficient for comparison to model-scale (here, 0.25°) estimates [19]. For these reasons, land surface property retrieval is considered beyond the scope of this study.

An important caveat of the study is that retrievals of MWE are themselves subject to considerable error. Inter-comparisons [3, 50, 51] of MWE retrieval products generated by a range of research groups using different, and in some cases even the same, instruments (SSM/I, TMI, and AMSR-E) have revealed significant differences. Even for relatively homogeneous scenes such as desert or rainforest, *mean* emissivity at GPM-relevant frequencies can vary up to 0.04 or higher across products [50, 51]. Likely error sources at lower frequencies include the surface skin temperature not being representative of that of the emitting soil layer [52–57], and at higher frequencies, errors in atmospheric profile data [57]. As such, the error statistics reported here should be viewed more as a test of whether it is viable to bring the model predictions and retrievals into better agreement through the calibration process than as a confirmatory statement on the value of the calibrated forward models. We therefore report root-mean-square-*difference* (RMSD) rather than RMSE. A MWE benchmark dataset, based on *in situ* measurement, is needed to fully validate the forward models along with the retrievals.

The RMSD of MWE forward model estimation at the time of AMSR-E overpasses, approximately 2 P.M. and 1 A.M. local time in the SGP, is evaluated for the following approaches to MWE estimation:

1. Forward modeling without calibration
2. Forward modeling with calibration
3. 1) and 2), after bias-correction
4. Daily climatology (based on MWE retrievals)

These results are further broken down by land cover class. Finally, to evaluate the worth of the joint LSM-MEM calibration, the percent change in RMSD is reported for LSM-only calibration and MEM-only calibration.

Methods and Data

LIS facilitates studies of the land surface and coupled systems through an object-oriented, interoperable high performance-computing software architecture [31, 32]. The object-oriented design enables the interchange of physical models, meteorological and model parameter datasets, and data assimilation methods. In addition, it supports the coupling of LSMs to a range of models. For example, LSMs can be coupled to meteorological models (e.g., the Weather and Research Forecasting (WRF) system), routing models, radiative transfer models (RTMs) and, the focus here, MEMs. Important to this study, LIS also includes an optimization and uncertainty estimation subsystem (LIS-OPT/UE) [18, 58], used here for the joint LSM-MEM calibration. LIS can be run at a user-designated spatial and temporal resolution. Here, the forward models are run hourly at 0.25°×0.25° over the SGP.

The overall forward modeling and calibration approach, as implemented within LIS, is depicted in Figure 1. Each solid box (e.g., “LSM”, “MEM”) refers to a software abstraction; implementation of the required interfaces associated with an abstraction defines a new instance (e.g., “Noah”, “CRTM”). The arrows indicate the passing of information between these abstractions. Below, we describe the methods and data in relation to Figure 1, starting with the *Forward model*.

LSMs simulate surface energy and water fluxes and budgets. Here, for consistency with previous land MWE studies [2, 3], Noah [59–61] version 3.3 was selected. The Noah LSM was originally developed from the land component of the Oregon State University 1-D planetary boundary layer model [62]. It is currently employed as the land surface scheme in NCEP’s global and regional operational models, including the Global Forecasting System (GFS), and the NCEP Weather Research and Forecasting Nonhydrostatic Mesoscale Model (WRF-NMM). The modeling of soil moisture in the Noah LSM, which has been extensively evaluated [14, 63], is handled by a formulation of the Richards’ equation governed by the Campbell [64] functions, with the soil profile discretized into 4 layers in the standard configuration, with a top layer of 10 cm.

Noah, and LSMs generally, are driven by near-surface atmospheric forcings (e.g., temperature, humidity, wind speed, precipitation). Here, downward shortwave and longwave

radiation, air temperature, specific humidity, wind speed and surface pressure are obtained from the North American Land Data Assimilation System (NLDAS2). NLDAS2 is generally regarded as a high quality forcings dataset for the continental United States (CONUS) as it incorporates data and analysis that are not available in real-time (e.g., gauge observations of precipitation, adjustments for topographical influences on precipitation, further quality control checks, downscaling)[65]. As a result, NLDAS2 can be expected to be of relatively higher quality than forcings datasets with global coverage.

LSM simulations depend on a wide range of parameters, including radiative parameters (e.g., albedo, emissivity), vegetation parameters (e.g., vegetation fraction, minimum stomatal resistance, leaf area index), thermal properties (e.g., quartz content), and soil hydraulic properties (e.g., porosity, hydraulic conductivity). Monthly, climatologically-derived values of albedo from NCEP are applied. While monthly climatological estimates of green vegetation fraction (*gvf*, the Noah variable SHDFAC) are typically used, given the importance of vegetation to the modeling of MWE, the 8-day Leaf Area Index (LAI) product from MODIS Collection 5 (MCD15A2.005)[66] is applied, with the raw 1km data gridded to the 0.25° running resolution. The product is only nominally 8-day as persistent cloud cover can result in interpolation between observations further than 8 days apart. To obtain *gvf*, we apply the conversion of Niu [67]:

$$gvf = 1 - \mathrm{e}^{-\mathrm{k}_{\mathrm{lai2vgf}} * LAI} \quad (1)$$

where k_{lai2vgf} is 0.52.

As noted in the introduction, most parameters in Noah (and other LSMs) are typically specified via lookup tables based on soil texture or land cover. Soil texture and vegetative land cover dominant at the 0.25°×0.25° running resolution is shown for the SGP (34°N: 39°N, 100°W:95°W) in Figure 2. The soil texture, as well as the underlying sand, clay, and silt fractions that serve as the direct inputs to the models, is drawn from the State Soil Geographic Database (STATSGO) maps [68]. Loams are the major soil texture type: *Silt Loam* (41% of pixels), *Sandy loam* (21%), followed by *Loam* (13%), *Silty clay loam* (13%), and *Clay loam* (5%). Other less represented soils include *Sand* (6%), *Clay* (1%) and *Silty Clay* (0.25%).

There is considerable variation in dominant land cover in the SGP (Figure 2; bottom). Of the thirteen land cover types in the Hansen et al. [69] classification, nine are represented. *Cropland*, defined as crops occupying more than 80% of the landscape, is the most prevalent (43% of pixels). As MWE has been shown to be sensitive to crop type [70, 71], we note that winter wheat represents approximately a third of all harvested (cultivated and non-cultivated) crops in the SGP according to the 2007 Census of Agriculture; west of 97W, by acreage it is the predominant crop. Corn, soybeans, and sorghum together represent an additional third, and Hay, which is harvested nearly uniformly in all but the northwestern corner of the SGP, represents the final third. Even where *Grassland* (22% of pixels) and *Wooded Grassland* (21%) dominate, *Cropland* is typically the second dominant land cover class in these areas, including the majority of the *Grassland* pixels shown in Figure 2, and,

north of 37°N, most of the *Wooded Grassland* pixels. The remaining land cover in the SGP is *Woodland* (6%) and *Closed Shrubland* (5%), and less than 2% each of *Evergreen Needleleaf Forest*, *Deciduous Broadleaf Forest*, *Mixed forest*, and *Urban and Built* areas. The two *Urban and Built* pixels correspond to the cities of Wichita, Kansas and Tulsa, Oklahoma.

The LSM-MEM interface (see Figure 1) specifies the mapping of the outputs of the LSM to the inputs of the MEM. At each of the hourly time steps, the LSM passes through or computes the variables needed by the MEM. For example, sand and clay fraction, and LAI, are passed through to the MEM. Soil moisture and soil temperature and other state variables are computed. The MEM then takes these inputs and generates estimates of MWE for different frequencies and polarizations (*SIM* in Figure 1) using parameterizations that capture the sensitivity of MWE to soil moisture, the effects of surface roughness, and the scattering effects and emission of vegetation (and snow).

Both MEMs were designed for global operations. For computational tractability, and in recognition of data limitations, their development invoked lower-order approximations of the radiative transfer equations [72]. For example, over vegetated surfaces both adopt the “tau-omega” model that is limited in its ability to capture multiple scattering and radiometrically important vegetation characteristics (e.g., leaf shape, size and orientation) [72–76]. Several [74, 77], however, have recognized that despite these simplifications, with adjustments to parameter values, the tau-omega model can often reasonably mimic more complete solutions, for example with the lowering of albedo to capture the darkening that results from multiple scattering. The identification of these “effective” parameter values has been achieved in two ways, either with tuning to a more complete radiative transfer solution [74] or, the approach taken here, with tuning to MWE observations [77].

CRTM is one component of a comprehensive, modular radiative transfer modeling system developed by the NOAA/NASA/DoD Joint Center for Satellite Data Assimilation (JCSDA). The version of CRTM used in this study is CRTM REL-2.0.2. CRTM is designed to simulate specific satellite-based sensors and, as such, is equipped to conduct radiative transfer calculations for a broad set of frequencies including infrared, visible, and microwave. Here, only that portion of CRTM that computes land surface MWE is invoked. The NESDIS_LandEM_Module developed at NOAA’s Environmental Satellite and Information Service (NESDIS), now referred to as the CRTM Surface Emissivity Model for Microwave (CSEM-MW)[78], is applied. Land MWE is simulated using a two-stream radiative approximation [15]. Reflection and emission occurring at the interfaces above and below the scattering layer (i.e., vegetation, snow) are incorporated. The cross polarization is expressed as a function of roughness height and frequency [79]. The input vegetation parameters are used to derive the absorption and scattering coefficients, which are then used in the tau-omega model to simulate the effect of vegetation cover [80]. Inputs relevant to snow-free MWE calculation are the satellite zenith angle, MW frequency, soil moisture content, vegetation fraction, soil temperature, and land surface skin temperature. We refer to the forward model approach involving CRTM as Noah-CRTM to make the dependency of the simulated MWE on the LSM explicit.

The second MEM used is CMEM [16, 17, 27], version 3.0. CMEM was designed to support radiative transfer calculation at lower microwave frequencies only (1 to 20 GHz). In this study we present results above 20 GHz but these should be considered "experimental" only. CMEM is similar to CRTM in that it contains modules for both surface MWE and atmospheric transfer calculations and relies essentially on the same physical principles for MWE calculation. In contrast, though, CMEM includes several optional modules for testing alternative empirical relationships and parameterization schemes, for example, for absorption and scattering [16, 17]. For this study, we have generally followed the choices made by Drusch [27]. As with CRTM, to reflect the dependency on the LSM, we refer to Noah-CMEM (rather than CMEM).

In this study, two choices related to the vegetation modeling are made that affect the MEM modeling. First, we introduce a simple coefficient, WATER_CONTENT_PER_LAI, that recognizes MODIS LAI as an, albeit limited [81], proxy measure of vegetation water content. Second, for the purposes of MWE estimation, each pixel is considered mixed in a two-component scene model, consisting of a bare ground and homogenously vegetated fraction. This strategy, which is similar to that used in the vegetation index/LAI literature [82, 83], recognizes the limitations of applying an average LAI value to a pixel due to the nonlinearities in the response of MWE to soil moisture and vegetation. Here, the bare ground fraction consists of a fixed, year-round bare ground fraction (bgf_{fixed}) and, using the Niu [67] relationship (Eq. 1), a variable bare ground fraction. The vegetated fraction is computed as earlier (Eq. 1), but applied only to the area that is not permanent bare ground, and therefore with an inflated LAI (factor: $1/(bgf_{fixed})$). At each time step, the MEM is run twice, once for the vegetated fraction and once for the bare ground fraction, with appropriate averaging. The motivation for this simplified approach over a more compute-intensive tiling approach, is general recognition of the significant limitations of the data and models, and indications that even at fine scales the mixed pixel problem is not avoided [84].

The calibration was conducted with LIS-OPT/UE [18, 58]. The LIS-OPT/UE subsystem provides a computational infrastructure that facilitates the application of parameter estimation and uncertainty estimation algorithms to the LIS land surface and coupled models. Here, we are invoking the LIS-OPT subsystem to conduct parameter estimation. As shown in Figure 1, the LIS-OPT subsystem *Optimization Algorithm* guides the search for "decision variables", here the model *Parameters*, in a direction of improvement in match between *SIM* and *OBS*, where the quality of the match is defined by an *Objective Function.*

The *Parameters* to be optimized are given in Table 1. As noted in the introduction, the parameter estimation is conducted "locally". The set of parameters requiring tuning is denoted as $\theta_{i,j}$ where i and j refer to the row and column, respectively, of the grid cell within the 0.25° SGP domain. The parameters to be tuned also include k_{lai2vgf}, which determines gvf as a function of LAI (Eq. 1), and, given its uncertainty and variation by land cover [81], WATER_CONTENT_PER_LAI that determines vegetation water content.

The inclusion of the LSM parameters results in a much larger set of parameters requiring tuning. For comparison, Drusch et al. [27] limited calibration to selection from among three parameterization schemes, and adjustment of three CMEM parameters—soil roughness,

vegetation structure coefficient, and vegetation water content for dense vegetation. In [28–30], five physical process parameters were tuned: two surface roughness-related parameters (describing surface roughness and its angular dependence), two vegetation structure-related parameters (relating vegetation optical thickness to LAI), and scattering albedo. Still a greater number of parameters could in principle be tuned, leading to a superior calibration, as there are numerous parameters not accessible through top-level interfaces, a point recently made for LSMs [41], and also certainly the case for MEMs.

The *OBS* in Figure 1 derive from the SGP cloud-cleared AMSR-E MWE retrievals of Ringerud et al. [2], the details of which are provided in that study. The retrievals were performed using level 1 C AMSR-E brightness temperatures under "Confident Clear" conditions in all 1-km MODIS pixels within the AMSR-E largest footprint. The retrievals also relied on space and time-interpolated ECMWF interim reanalysis (ERA-Interim) 3-hourly, 1-degree surface skin temperature and water vapor. The retrieval scheme involved radiative transfer modeling in an iterative procedure to determine the surface microwave emission best matching predicted and AMSR-E-observed brightness temperatures.

We restrict the observations used in the calibration to low frequency channels to avoid the atmospheric contamination errors of the higher frequency channels [50]. Five different sets of low frequency channels, C, were tested: (6.925H), (6.925V), (6.925H,10.65H), (6.925V, 6.925H), and (10.65V, 10.65H). We present only the results of C=(10.65V,10.65H) as the conclusions of this study were insensitive to the selection of calibration channel combination, and as (10.65V,10.65H) was a slightly better performer; differences (after bias correction) were less than 1% in RMSD. In the validation, the model uses the calibrated parameters to predict at all channels.

To obtain a retrieval estimate more commensurate with the 0.25° model-based estimates, the retrievals were processed beyond that done by Ringerud [2] to improve the quality of the calibration dataset. For each overpass, the retrievals were geo-located into the grid cells based on the lat/lon center points. If there were at least five retrievals falling within the 0.25° grid cell for that overpass, then the retrieved MWE was averaged to obtain the grid cell estimate; otherwise the average was presumed to lack sufficient accuracy for the purposes of calibration (and validation). In addition, as the scope of this study was restricted to the MWE dynamics of the soil-vegetation system, if at the time of overpass any of the models indicated a land surface or soil temperature below 275° K, or snow, the retrieval was excluded. The number of retrievals varied greatly within the year, and from year to year, with far fewer retrievals in the months of December through February due to the cloud masking and conservative masking for frozen ground and snow.

The calibration period was selected to be the warm season of 2008, defined as being from April 1, 2008 through September 30, 2008. The year 2008 was selected as in other SGP studies it was deemed more moderate than the anomalously dry 2006 and anomalously wet 2007 [26, 85]. Calibration was restricted to the warm season to avoid frozen soil and snow. For the grid cell at row i and column j, we refer to the retrieval for channel c at model time step t as $y_{t,c,i,j}$. The full set of time steps of retrievals, which correspond to the cloud-cleared, snow and frozen ground-free descending and ascending overpasses, for the calibration

period is referred to as T and, as earlier mentioned, the full set of channels calibrated to as C, with here C=(10.65V,10.65H). The forward model-simulated emissivities (SIM in Figure 1) using trial parameter set $\theta_{i,j}$ are denoted by $\varepsilon_{t,c,i,j}(\theta_{i,j})$.

As in other LSM and MEM calibration studies [23–25, 86], the familiar least squares *Objective Function* is applied. The following problem was solved for each grid cell:

$$\min_{\theta_{i,j}} Z = \sum_{t \in T} \sum_{c \in C} w_C * (\varepsilon_{t,c,i,j}(\theta_{i,j}) - y_{t,c,i,j})^2 \quad (2)$$

Each channel c in C was equally weighted, i.e., w_c=1. The resulting least squares solution can be viewed as a maximum likelihood solution if the residuals $\varepsilon_{t,c,i,j}(\theta_{i,j}) - y_{t,c,i,j}$ can be described by an independent and identically distributed (iid) normal error model [87].

A genetic algorithm was selected as the *Optimization Algorithm* to solve the above optimization problem (Eq. 2). Genetic algorithms are stochastic, global search algorithms that draw on concepts from evolutionary search, mimicking the process of natural selection [88]. They are particularly suited to challenging problems like parameter estimation in which the objective function response surface may not be smooth and may have multiple local optima, properties that can confound deterministic (e.g., gradient-based) search algorithms. The genetic algorithm within LIS is described in detail in Kumar [58]. The particular configuration used here relies on a population size of 20, a mutation rate of 2%, 90% crossover rate, elitism, and a two-point crossover scheme.

In all calibration (and default) runs, the Noah LSM was run over a two-year spin-up period to obtain the land surface states (e.g., soil moisture, soil temperature) just prior to the calibration period. The spin-up is a typical land surface modeling practice that allows for the land surface states at the beginning of the period of interest to become independent of the guess states at the start of the spin-up period. The additional two years of simulation greatly adds to the computation time but is necessary as the spun-up initial land surface states are impacted by changes to the parameters (e.g., maximum soil moisture). After finding the genetic algorithm solutions to Eq. 2, i.e., the models are run over the validation period using the “optimal” parameter values $\theta_{i,j}$* . The approximately seven-year validation period consists of the AMSR-E period of record less the two-year spin-up and six-month calibration period.

The daily climatological estimates, which provide an additional point of reference, were developed in the following way. For each grid cell and AMSR-E channel, climatological monthly means were computed using retrievals developed over the AMSR-E record. Daily estimates were arrived at by interpolating between the climatological monthly means, each pinned to the 15th day of the month.

Results & discussion

Below, the forward model performance over the 7-yr validation period is discussed. Root-mean-square-difference (RMSD) is the metric selected to evaluate consistency with the AMSR-E retrievals. For readability, in the tables and text RMSD*100 is reported.

In Table 2, RMSD*100 was computed for each frequency, for both the calibrated and un-calibrated models. To differentiate results in the figures and text when discussing the calibrated models, we append “C-” to the model name, e.g, C-Noah-CRTM and C-Noah-CMEM. Also, given atmospheric contamination in retrievals particularly at 89V and 89H, averages including and excluding 89 are supplied.

First we consider the RMSD of Noah-CRTM and Noah-CMEM prior to calibration. Noah-CRTM and Noah- CMEM outperform climatology only at 10.65H. The lack of agreement with retrievals is as observed in prior studies [2, 50]. Noah-CRTM is more consistent with retrievals than Noah-CMEM. As averaged across all channels, RMSD*100 computed for Noah-CRTM was 2.4, more than 40% less than that of Noah-CMEM, 4.2. The maximum RMSD across channels was 3.4 for Noah-CRTM as compared to 6.0 for Noah-CMEM.

After calibration, the model estimates are much more consistent with the retrievals, with C-Noah-CRTM remaining better in terms of RMSD. C-Noah-CRTM achieves an RMSD*100 of 2.2, whereas that of C-Noah-CMEM remains higher, 2.9. The improvement in RMSD from calibration is considerable. The extent of improvement was slighter for C-Noah-CRTM, with RMSD*100 decreasing from 2.4 to 2.2, as compared to C-Noah-CMEM, which decreased from 4.2 to 2.9. Excluding 89 from results, C-Noah-CRTM remains superior, with an average RMSD*100 of 1.8, as compared to C-Noah-CMEM’s 2.1.

The high average RMSD of C-Noah-CMEM is a result of performance at the higher frequency channels, with C-Noah-CMEM quickly degrading to 3.7 at 36.5H and 6.0 at 89.0H. This is perhaps a result of CMEM’s design focus on frequencies only up to 20 GHz. At the lower frequency channels, 10.65 to 18.7, C-Noah-CMEM generally outperformed C-Noah-CRTM, only worse at 10.65V.

At the lower frequencies, calibration had the effect of removing the large emissivity simulation differences between the models. This is nicely summarized by the plot (Figure 3) of the probability density functions, or “PDFs”, of 10.65H GHz MWE for the un-calibrated and calibrated models, which were generated using all points in the domain. Noah-CMEM systematically simulated emissivities much lower than Noah-CRTM. These differences are mostly erased with calibration, with the mode of C-Noah-CMEM only slightly lower, by about 0.01 emissivity, than that of C-Noah-CMEM, and with virtually no differences at the low-emissivity end of the PDF.

Also shown in Figure 3 are the PDFs for the retrievals at 10.65H GHz. It can be seen that the un-calibrated Noah-CMEM emissivities are much lower than the retrievals, which was driving the large RMSD (as opposed to simply large random errors). But post calibration, the models are much more consistent with the retrievals. However, the dynamic range in MWE of the calibrated models is clearly narrower than that of the retrievals.

A number of factors may be contributing to the narrower dynamic range of the model emissivities post calibration. Errors in the emissivity retrievals themselves stemming from incorrect values of surface temperature are one source [3, 50, 51, 53]. The surface temperatures used in the retrievals will depart from the effective temperature of the emitting soil layer at 10.65 GHz at the AMSR-E overpass times (about 2PM and 1AM local in the SGP), and in particular at the time of the afternoon overpass [89]. In addition, the dependence of the effective depth of the emitting soil layer on soil moisture is a complicating factor.

The narrower PDF may also reflect inadequate physics for the LSM or MEM. For example, LSMs, including Noah v3.3, lack the ability to capture inundation, which has the effect of greatly reducing emissivity and increasing polarization. Within the calibration period, there was extreme precipitation from September 11-15, 2008 from a continental-type storm event (12-inch rain in parts of Kansas) followed by the remnants of a hurricane [90]. And within the validation period, specific locations experienced serious flooding on April 28, 2009. The retrieved microwave polarization difference index (MPDI) and emissivities at these points and times were consistent with inundation [91, 92]. To fully explore the effects of inundation on the calibration, ancillary datasets (e.g., scatterometer) would be needed as passive microwave alone is not sufficient to indicate flooding, as different mixed scenes of open water and wet soils present similar MWE signatures [91, 93, 94].

Also, limitations in the MEM physics may be a contributing factor. For example, CRTM and CMEM apply the same roughness value to all frequencies and polarizations. Several have investigated roughness parameterizations that have frequency dependence [95] and that also introduce dependency on soil moisture [96–98]. In addition, the models do not account for phenomena such as dew or intercepted water, both of which can exert influence over emissivity, including, it is thought, in the SGP [99]. To improve the models, these issues need further exploration.

The calibration moved both models towards a generally drier state to increase MWE sensitivity to soil moisture changes. MWE is more responsive to addition of water to dry soils rather than wet soils. PDFs for soil moisture (Figure 4) illustrate this point. The PDFs were generated for the domain, both before and after calibration, using all points in the SGP. Calibration had the effect of shifting both model's estimates of soil moisture towards a generally drier state. The PDF mode of C-Noah-CRTM and C-Noah-CMEM, respectively, was approximately two-thirds and one-third that of Noah left un-calibrated. While this change in soil moisture is large, it is well within the range of biases reported for Noah and other LSMs, including in the Great Plains (e.g.,[14]).

The validity of the both C-Noah-CRTM and C-Noah-CMEM soil moisture estimates across the SGP is generally unknown. The soil moisture estimates were not compared to products based on AMSR-E or other passive microwave instruments as these products cannot be considered independent as they, too, rely on similar modeling (typically without calibration). One of the few grid cells for which spatially averaged *in situ* soil moisture data is believed to be fairly representative is for the single grid cell (34.875°N, 98.125°W) that corresponds to the USDA Agricultural Research Service (ARS) Little Washita River Experimental

Watershed [55, 100, 101]. The grid cell encompasses a large fraction of the experimental watershed. Land cover consists of pasture and rangeland, and winter wheat. The soil moisture time series (Figure 5) illustrates that the drying out brought about by calibration is warranted, as the in situ data are much drier than Noah left uncalibrated. In addition, the time series indicates differences in dynamic range and rate of dry-down for the calibrated models, behaviors seen in many such time series across the SGP. C-Noah-CMEM exhibits a wider dynamic range and faster dry-down than C-Noah-CRTM, which appears more consistent with the in situ data. However, both models continue to exhibit a wet bias with respect to the *in situ* data.

The adjustment in the models' simulation of soil moisture was accompanied by simultaneous changes in the sensitivity to LAI. Differences between the calibrated models are evident when examining MWE as a function of soil moisture and LAI. The average MWE for bins of soil moisture and LAI are shown in Figure 6 for 10.65H, for the un-calibrated models (Figures 6a,6b) and the calibrated models (Figures 6d,6e). Were the models to exhibit the same behaviors, we would expect the plots to be very similar. However, referring to Figures 6d and 6e, at high values of soil moisture and at LAI around 3, the MWE response is markedly different. In this region, in these average terms, C-Noah-CRTM shows MWE sensitivity to soil moisture, whereas C-Noah-CMEM does not. A caveat of these MWE-soil moisture-LAI plots is that they indicate only *average* MWE, lumping together many different SGP locations, each of which has its own optimal parameter set and therefore unique MWE-soil moisture-LAI relationship, and which generally occupies only a limited portion of the soil moisture-LAI space shown.

Also in Figure 6, the MWE-soil moisture-LAI plots are shown for the retrievals. Prior to calibration, the plots for both models (Figures 6a,6b) are quite different as compared to the retrievals (Figure 6c). For the case after calibration, two plots are needed to show the retrievals' sensitivity to soil moisture and LAI, as the calibration affects the soil moisture modeling on the x-axis. By comparing each model's plot with the respective retrievals plots (i.e., Figure 6d and 6f, and 6e with 6f), two observations can be made. First, the distinct patterns seen for each model are largely replicated in each corresponding retrievals plot. As a consequence, absent other information, no one model appears more consistent with the retrievals than the other at 10.65H. Second, in comparison to the retrievals, both tend to overestimate MWE in very dry conditions, and exhibit too little soil moisture sensitivity at values of LAI near 1 and below. The overly high MWE in dry conditions is more evident with C-Noah-CRTM than C-Noah-CMEM, whereas the low sensitivity to soil moisture at low LAI is more evident with C-Noah-CMEM. It is not clear why. The general appearance of the plots for calibrated C-Noah-CMEM appear consistent with those of [13], which, while showing vegetative water content in place of LAI, indicate little emissivity sensitivity to soil moisture at all but the lowest level of vegetation.

Next, we applied a simple bias correction to the model estimates. This was motivated by the earlier observation of the smaller dynamic range as compared with retrievals (Figure 3), and also motivated by having observed significant anomaly correlations (not shown) in the *Cropland* and *Grassland* land cover classes. For each grid cell, month, and channel, linear regression was applied with the retrievals as the dependent variable and model estimate as

the independent variable. To put on an equal footing with the climatology, the full set of observations used in the development of the climatological estimates was used in the linear regression. By doing so, this approach also partially addresses in the comparison any systematic biases in the retrievals themselves (e.g., surface temperature and emitting-layer temperature mismatch at lower frequencies, atmospheric contamination at higher frequencies).

The results (Table 3) indicate that use of the models would improve upon climatology to a significant degree. Even if left un-calibrated, once bias-corrected, there is improvement. The across-channel-average RMSD*100 for Noah-CRTM and Noah-CMEM, respectively, is 1.40 and 1.42, a 14% and 13% reduction from that of climatology (excl. 89 GHz: 17% and 14%). Calibration leads to further improvements. The across-channel-average RMSD*100 was 1.36 and 1.32 for C-Noah-CRTM and C-Noah-CMEM, a 17% and 19% reduction from climatology (excl. 89 GHz: 21% and 25%). Thus, incorporating calibrated forward model estimates of the dynamics of MWE, after correcting for systematic biases through linear regression, can result in approximately a 20% channel-average reduction in RMSD as compared to reliance on climatology.

In Table 4, we show RMSD for bias-corrected C-Noah-CRTM and C-Noah-CMEM by land cover class. C-Noah-CRTM and C-Noah-CMEM are in general agreement. *Evergreen Needleleaf Forest* has the lowest RMSD*100, 1.02 and 1.01, respectively for C-Noah-CRTM and C-Noah-CMEM (excluding 89 GHz, 0.72 and 0.71). *Cropland*, the predominant land cover class in the SGP, has the highest, 1.44 and 1.39 (excl. 89 GHz, 1.24 and 1.19). Overall, the models, once calibrated, and after addressing the bias, are very similar, and appear almost interchangeable.

The percentage change in RMSD from climatology is also listed In Table 4. For forested land cover (*Evergreen Needleleaf Forest*, *Deciduous Broadleaf Forest*, *Mixed Forest* and *Woodland*), the reduction is small, less than 10%. This is followed by *Wooded Grassland, Closed Shrubland, Grassland*, and *Cropland.* The percentage reduction from climatology is smaller for Noah-CRTM than Noah-CMEM for these classes. For *Cropland*, RMSD is reduced by 20% and 23% for Noah-CRTM and Noah-CMEM, respectively (excl. 89 GHz: 26% and 29%). For the *Urban and Built* land cover class, calibration reduces RMSD by about 10% from climatology.

We next explore the losses, if any, of calibrating only the LSM or only the MEM. As mentioned in the introduction, for understandable reasons, e.g., so as not to upset the land surface model climatology given the range of uses of the models, typically the MEM alone has been calibrated with the LSM left unchanged, e.g.,[28, 29]. The risk of restricting the calibration only to the MEM is that the issue with soil moisture dynamic range that was identified by [27, 30] is not properly addressed. It is therefore important to know the extent of any potential gains of joint calibration, which we briefly address here.

In Table 5, for each model, the change in RMSD is shown when calibrating only the LSM or only the MEM. With the exception of 89.0V/H, RMSD is higher if not performing joint calibration. Excluding 89.0V/H, for C-Noah-CRTM, RMSD is as much as 10% higher, and

for C-Noah-CMEM, as much as 22% higher. For C-Noah-CRTM and C-Noah-CMEM, respectively, the increase in the average RMSD (excluding 89GHz) is 2.3% and 2.7% for LSM-only calibration, and 5.5% and 12% for MEM-only calibration. This would suggest that for MWE estimation it is more important to calibrate the LSM than the MEM. For these results, the bias-corrected model estimates were used. Absent bias correction, the results (not shown) are similar but amplified, with the percentage change in RMSD at lower frequency channels significantly higher.

Conclusions

Improving the accuracy of forward model-simulated land microwave emissivity would be beneficial as retrieving precipitation over land requires removal of the land background signal. Prior studies, however, have highlighted the limited predictive power of forward models for microwave emissivity estimation. This study evaluated the potential for improving forward modeling through calibration to address the problem of poor model parameter specification.

The goal of the calibration exercise was to maximize the closeness of forward model predictions of microwave emissivity with retrieved estimates of emissivity during snow-free, unfrozen conditions. The domain selected was the U.S. Southern Great Plains (SGP). CRTM (version 2.0.2) and CMEM (version 3.0), two microwave emissivity models, both taking inputs from the Noah land surface model (version 3.3), formed the two basic model configurations that were subjected to the calibration. AMSR-E cloud-cleared retrievals for channels very similar to those of GPM were used for calibration and validation. An optimization method (genetic algorithm) was applied to search for the values of thirty-five land surface and microwave emissivity model parameters minimizing the familiar “least squares” criterion.

Calibration improved the agreement of the forward model and retrieved estimates of microwave emissivity. The calibration of Noah-CRTM and Noah-CMEM resulted in drier soil moisture states being simulated (more so for Noah-CMEM) and with simultaneous adjustments to vegetation sensitivity. Calibrated Noah-CMEM resulted in a better match to the retrievals at lower frequency channels than Noah-CRTM (RMSD as averaged over 10.65 GHz and 18.7 GHz channels, V and H polarizations: Noah- CRTM, 0.0089; Noah-CMEM=0.0087), but a worse match overall due to high RMSD at high frequency channels (RMSD as averaged over all channels : Noah-CRTM, 0.022; Noah-CMEM=0.029), though it is important to note that CMEM is designed only up to 20 GHz. A systematic bias of the calibrated forward models was observed, a distinctly narrower dynamic range than the retrievals. Possible explanations include surface temperature errors in the retrievals, a lack of an inundation modeling ability in land surface models, and limitations in the models’ roughness parameterization schemes.

A bias correction scheme was applied to the model estimates, as would be done if implementing the models in operations. This led to a much better match to retrieved emissivities. The average RMSD for both forward models was just over 0.013, which compared to before bias correction represents a one-third and one-half reduction for Noah-

CRTM and Noah-CMEM, respectively. This also represents an approximate 10% improvement over the models when left un-calibrated but bias-corrected.

Use of the forward models to capture the dynamics of emissivity can lead to improvements over reliance on daily climatology (as interpolated from monthly emissivity climatology). In average terms, the models achieve an approximate 20% reduction in RMSD over climatology.

The improvements in RMSD differed by land cover. RMSD (after bias correction) was least for forested areas in absolute terms (0.010) and in percentage reduction from climatology (<10%). RMSD was highest for grasslands and cropland in absolute terms (0.014) and percentage improvement (near 20%).

Numerous calibration exercises were performed. Joint calibration of the land surface and microwave emissivity model was found to result in lower RMSD than calibrating only the microwave emissivity model, which was the approach taken in previous related calibration studies. The calibration of the microwave emissivity model alone resulted in RMSD that was 6% and 12% higher than the joint calibration for Noah-CRTM and Noah-CMEM, respectively. Land surface model-only calibration resulted in approximately 2% higher RMSD for both models. In another calibration exercise, the study conclusions were found to be insensitive to the choice between five different channel combinations against which to calibrate (bias-corrected RMSD <1% difference). Calibration to 10.65 GHz V and H, equally weighted, proved adequate.

The validation of the calibrated forward models depends on high quality calibration datasets, particularly. A sound *in situ*-based emissivity dataset would help in discerning the source of discrepancies between the forward models and retrievals, both of which are subject to error. The availability of sound datasets would also help to guide model development.

With further development, the forward models, with their ability to capture the dynamics in microwave emissivity, could improve the accuracy of overland precipitations in the GPM-era. However, further studies are needed to quantify the impact of improved emissivity estimation on precipitation retrieval accuracy, and ultimately on the applications (e.g., water budgets, flooding, drought, landslide assessment) that rely on precipitation retrievals.

Acknowledgments

This research is supported by the National Aeronautics and Space Administration Precipitation Science Program under Solicitation NNH09ZDA001N (PI: C. D. Peters-Lidard), and is part of the GPM Land Surface Working Group activities organized by Ralph Ferraro, Christa Peters-Lidard and F. Joe Turk. Computational support was provided by NASA Center for Climate Simulation (NCCS). Helpful discussions with Mehmet Kurum, Ed Kim, Alicia Joseph, Peggy O'Neil and Scott Rheingrover are appreciated. Also, we thank Pat Starks and Michael Cosh of USDA-ARS. Finally, we thank the anonymous reviewers for their detailed comments and suggestions.

References

1. Hou AY, Kakar RK, Neeck S, Azarbarzin AA, Kummerow CD, Kojima M, et al. The Global Precipitation Measurement Mission. Bulletin of the American Meteorological Society. 2014; 95:701–722. 2014/05/01.

2. Ringerud S, Kummerow C, Peters-Lidard C, Tian Y, Harrison K. A Comparison of Microwave Window Channel Retrieved and Forward-Modeled Emissivities Over the U.S. Southern Great Plains. Geoscience and Remote Sensing, IEEE Transactions on. 2014; 52:2395–2412.
3. Ferraro RR, Peters-Lidard CD, Hernandez C, Turk FJ, Aires F, Prigent C, et al. An Evaluation of Microwave Land Surface Emissivities Over the Continental United States to Benefit GPM-Era Precipitation Algorithms. Geoscience and Remote Sensing, IEEE Transactions on. 2013; 51:378–398.
4. Kummerow CD, Hong Y, Olson WS, Yang S, Adler RF, McCollum J, et al. The Evolution of the Goddard Profiling Algorithm (GPROF) for Rainfall Estimation from Passive Microwave Sensors. Journal of Applied Meteorology. 2001; 40:1801–1820. 2001/11/01.
5. Kummerow CD, Ringerud S, Crook J, Randel D, Berg W. An Observationally Generated A Priori Database for Microwave Rainfall Retrievals. Journal of Atmospheric and Oceanic Technology. 2010; 28:113–130. 2011/02/01.
6. Kummerow CD, Randel D, Kulie M, Wang N-Y, Ferraro R, Munchak SJ, et al. The Evolution of the Goddard Profiling Algorithm to a Fully Parametric Scheme. J Atmos Oceanic Technol. 2015 (in review).
7. Petty GW, Li K. Improved Passive Microwave Retrievals of Rain Rate over Land and Ocean. Part I: Algorithm Description. Journal of Atmospheric and Oceanic Technology. 2013; 30:2493–2508. 2013/11/01.
8. Petty GW, Li K. Improved Passive Microwave Retrievals of Rain Rate over Land and Ocean. Part II: Validation and Intercomparison. Journal of Atmospheric and Oceanic Technology. 2013; 30:2509–2526. 2013/11/01.
9. Aires F, Prigent C, Bernardo F, Jimenez C, Saunders R, Brunel P. A Tool to Estimate Land-Surface Emissivities at Microwave frequencies (TELSEM) for use in numerical weather prediction. Quarterly Journal of the Royal Meteorological Society. Apr.2011 137:690–699.
10. Turk FJ, Haddad ZS, You Y. Principal Components of Multifrequency Microwave Land Surface Emissivities. Part I: Estimation under Clear and Precipitating Conditions. Journal of Hydrometeorology. 2013; 15:3–19. 2014/02/01.
11. You Y, Turk FJ, Haddad ZS, Li L, Liu G. Principal Components of Multifrequency Microwave Land Surface Emissivities. Part II: Effects of Previous-Time Precipitation. Journal of Hydrometeorology. 2013; 15:20–37. 2014/02/01.
12. Ringerud S, Kummerow CD, Peters-Lidard CD. A Semi-Empirical Model for Computing Land Surface Emissivity in the Microwave Region. Geoscience and Remote Sensing, IEEE Transactions on. 2015; 53:1935–1946.
13. Turk FJ, Li L, Haddad ZS. A Physically Based Soil Moisture and Microwave Emissivity Data Set for Global Precipitation Measurement (GPM) Applications. Geoscience and Remote Sensing, IEEE Transactions on. 2014; 52:7637–7650.
14. Xia Y, Sheffield J, Ek MB, Dong J, Chaney N, Wei H, et al. Evaluation of multi-model simulated soil moisture in NLDAS-2. Journal of Hydrology. 512:107–125. 5/6/2014.
15. Weng FZ, Yan BH, Grody NC. A microwave land emissivity model. Journal of Geophysical Research-Atmospheres. Sep.2001 106:20115–20123.
16. Holmes TRH, Drusch M, Wigneron JP, de Jeu RAM. A global simulation of microwave emission: Error structures based on output from ECMWF's operational integrated forecast system. IEEE Trans Geosci Remote Sens. Mar; 2008 46(3):846–856.
17. de Rosnay P, Drusch M, Boone A, Balsamo G, Decharme B, Harris P, et al. AMMA Land Surface Model Intercomparison Experiment coupled to the Community Microwave Emission Model: ALMIP-MEM. Journal of Geophysical Research: Atmospheres. 2009; 114:D05108.
18. Harrison KW, Kumar SV, Peters-Lidard CD, Santanello JA. Quantifying the change in soil moisture modeling uncertainty from remote sensing observations using Bayesian inference techniques. Water Resources Research. 2012; 48:W11514.
19. Vereecken H, Kasteel R, Vanderborght J, Harter T. Upscaling hydraulic properties and soil water flow processes in heterogeneous soils: A review. Vadose Zone Journal. Feb.2007 6:1–28.
20. Schaap MG, Leij FJ. Using neural networks to predict soil water retention and soil hydraulic conductivity. Soil & Tillage Research. Jun.1998 47:37–42.

21. Gutmann ED, Small EE. A comparison of land surface model soil hydraulic properties estimated by inverse modeling and pedotransfer functions. Water Resources Research. May.2007 43
22. Deng HL, Ye M, Schaap MG, Khaleel R. Quantification of uncertainty in pedotransfer function-based parameter estimation for unsaturated flow modeling. Water Resources Research. Apr.2009 45
23. Santanello JA, Peters-Lidard CD, Garcia ME, Mocko DM, Tischler MA, Moran MS, et al. Using remotely-sensed estimates of soil moisture to infer soil texture and hydraulic properties across a semi-arid watershed. Remote Sensing of Environment. Sep.2007 110:79–97.
24. Peters-Lidard CD, Mocko DM, Garcia M, Santanello JA, Tischler MA, Moran MS, et al. Role of precipitation uncertainty in the estimation of hydrologic soil properties using remotely sensed soil moisture in a semiarid environment. Water Resources Research. May.2008 44
25. Gutmann ED, Small EE. A method for the determination of the hydraulic properties of soil from MODIS surface temperature for use in land-surface models. Water Resources Research. Jun.2010 46
26. Santanello JA, Kumar SV, Peters-Lidard CD, Harrison KW, Zhou S. Impact of Land Model Calibration on Coupled Land–Atmosphere Prediction. Journal of Hydrometeorology. 2013; 14:1373–1400. 2013/10/01.
27. Drusch M, Holmes T, de Rosnay P, Balsamo G. Comparing ERA-40-Based L-Band Brightness Temperatures with Skylab Observations: A Calibration/Validation Study Using the Community Microwave Emission Model. Journal of Hydrometeorology. 2009; 10:213–226. 2009/02/01.
28. De Lannoy GJM, Reichle RH, Pauwels VRN. Global Calibration of the GEOS-5 L-Band Microwave Radiative Transfer Model over Nonfrozen Land Using SMOS Observations. Journal of Hydrometeorology. 2013; 14:765–785. 2013/06/01.
29. De Lannoy GJM, Reichle RH, Vrugt JA. Uncertainty quantification of GEOS-5 L-band radiative transfer model parameters using Bayesian inference and SMOS observations. 2014; 148:146–157.
30. Lievens H, Al Bitar A, Verhoest NEC, Cabot F, De Lannoy GJM, Drusch M, et al. Optimization of a Radiative Transfer Forward Operator for Simulating SMOS Brightness Temperatures over the Upper Mississippi Basin. Journal of Hydrometeorology. 2015; 16:1109–1134. 2015/06/01.
31. Kumar SV, Peters-Lidard CD, Tian Y, Houser PR, Geiger J, Olden S, et al. Land information system: An interoperable framework for high resolution land surface modeling. Environmental Modelling & Software. Oct.2006 21:1402–1415.
32. Peters-Lidard CD, Houser PR, Tian Y, Kumar SV, Geiger J, Olden S, et al. High-performance Earth system modeling with NASA/GSFC's Land Information System. Innovations in Systems and Software Engineering. 2007; 3:157–165.
33. Schoups G, Vrugt JA. A formal likelihood function for parameter and predictive inference of hydrologic models with correlated, heteroscedastic, and non-Gaussian errors. Water Resources Research. Oct.2010 46
34. Hollenbeck KJ, Jensen KH. Maximum-likelihood estimation of unsaturated hydraulic parameters. Journal of Hydrology. Sep.1998 210:192–205.
35. Ines AVM, Mohanty BP. Parameter conditioning with a noisy Monte Carlo genetic algorithm for estimating effective soil hydraulic properties from space. Water Resources Research. Aug.2008 44
36. Doherty J, Welter D. A short exploration of structural noise. Water Resources Research. May.2010 46
37. Kuczera G, Kavetski D, Franks S, Thyer M. Towards a Bayesian total error analysis of conceptual rainfall-runoff models: Characterising model error using storm-dependent parameters. Journal of Hydrology. Nov.2006 331:161–177.
38. Kavetski D, Kuczera G, Franks SW. Bayesian analysis of input uncertainty in hydrological modeling: 1. Theory. Water Resources Research. Mar.2006 42
39. Kavetski D, Kuczera G, Franks SW. Bayesian analysis of input uncertainty in hydrological modeling: 2. Application. Water Resources Research. Mar.2006 42
40. Salamon P, Feyen L. Assessing parameter, precipitation, and predictive uncertainty in a distributed hydrological model using sequential data assimilation with the particle filter. Journal of Hydrology. Oct-15/;2009 376:428–442.

41. Mendoza PA, Clark MP, Barlage M, Rajagopalan B, Samaniego L, Abramowitz G, et al. Are we unnecessarily constraining the agility of complex process-based models? Water Resources Research. 2015; 51:716–728.
42. Wang H, Harrison K. Bayesian approach to contaminant source characterization in water distribution systems: adaptive sampling framework. Stochastic Environmental Research and Risk Assessment. 2013; 27:1921–1928. 2013/12/01.
43. Wang H, Harrison K. Bayesian Update Method for Contaminant Source Characterization in Water Distribution Systems. Journal of Water Resources Planning and Management. 2011; 139:13–22. 2013/01/01.
44. Harrison KW. Test application of Bayesian Programming: Adaptive water quality management under uncertainty. Advances in Water Resources. Mar.2007 30:606–622.
45. Harrison KW. Two-stage decision-making under uncertainty and stochasticity: Bayesian Programming. Advances in Water Resources. Mar.2007 30:641–664.
46. Sadegh M, Vrugt JA. Approximate Bayesian Computation using Markov Chain Monte Carlo simulation: DREAM(ABC). Water Resources Research. 2014; 50:6767–6787.
47. Thyer M, Renard B, Kavetski D, Kuczera G, Franks SW, Srikanthan S. Critical evaluation of parameter consistency and predictive uncertainty in hydrological modeling: A case study using Bayesian total error analysis. Water Resources Research. Apr.2009 45
48. Vrugt JA, Diks CGH, Gupta HV, Bouten W, Verstraten JM. Improved treatment of uncertainty in hydrologic modeling: Combining the strengths of global optimization and data assimilation. Water Resources Research. Jan.2005 41
49. Salamon P, Feyen L. Disentangling uncertainties in distributed hydrological modeling using multiplicative error models and sequential data assimilation. Water Resources Research. Dec.2010 46
50. Tian Y, Peters-Lidard CD, Harrison KW, Prigent C, Norouzi H, Aires F, et al. Quantifying Uncertainties in Land-Surface Microwave Emissivity Retrievals. Geoscience and Remote Sensing, IEEE Transactions on. 2014; 52:829–840.
51. Norouzi H, Temimi M, Prigent C, Turk J, Khanbilvardi R, Tian Y, et al. Assessment of the consistency among global microwave land surface emissivity products. Atmos Meas Tech. 2015; 8:1197–1205.
52. Norouzi H, Rossow W, Temimi M, Prigent C, Azarderakhsh M, Boukabara S, et al. Using microwave brightness temperature diurnal cycle to improve emissivity retrievals over land. Remote Sensing of Environment. Aug-/;2012 123:470–482.
53. Prigent C, Rossow WB, Matthews E, Marticorena B. Microwave radiometric signatures of different surface types in deserts. Journal of Geophysical Research-Atmospheres. May.1999 104:12147–12158.
54. Galantowicz JF, Moncet J-L, Liang P, Lipton AE, Uymin G, Prigent C, et al. Subsurface emission effects in AMSR-E measurements: Implications for land surface microwave emissivity retrieval. Journal of Geophysical Research: Atmospheres. 2011; 116:n/a–n/a.
55. Jackson TJ, Cosh MH, Bindlish R, Starks PJ, Bosch DD, Seyfried M, et al. Validation of Advanced Microwave Scanning Radiometer Soil Moisture Products. Ieee Transactions on Geoscience and Remote Sensing. Dec.2010 48:4256–4272.
56. Kerr YH, Njoku EG. A semiempirical model for interpreting microwave emission from semiarid land surfaces as seen from space. Geoscience and Remote Sensing, IEEE Transactions on. 1990; 28:384–393.
57. Hu Y, Fuzhong W. Error Sources in Remote Sensing of Microwave Land Surface Emissivity. Geoscience and Remote Sensing, IEEE Transactions on. 2011; 49:3437–3442.
58. Kumar SV, Reichle RH, Harrison KW, Peters-Lidard CD, Yatheendradas S, Santanello JA. A comparison of methods for a priori bias correction in soil moisture data assimilation. Water Resources Research. 2012; 48:W03515.
59. Mitchell, K. THE COMMUNITY Noah LAND-SURFACE MODEL (LSM) User's Guide Public Release Version 2.7.1. 2005. Jan 30. Available: http://www.emc.ncep.noaa.gov/mmb/gcp/noahlsm/Noah_LSM_USERGUIDE_2.7.1.htm

60. Ek MB, Mitchell KE, Lin Y, Rogers E, Grunmann P, Koren V, et al. Implementation of Noah land surface model advances in the National Centers for Environmental Prediction operational mesoscale Eta model. Journal of Geophysical Research-Atmospheres. Nov.2003 108
61. Chen F, Janjic Z, Mitchell K. Impact of atmospheric surface-layer parameterizations in the new land-surface scheme of the NCEP mesoscale Eta model. Boundary-Layer Meteorology. Dec.1997 85:391–421.
62. Troen I, Mahrt L. A SIMPLE-MODEL OF THE ATMOSPHERIC BOUNDARY-LAYER - SENSITIVITY TO SURFACE EVAPORATION. Boundary-Layer Meteorology. Oct.1986 37:129–148.
63. Robock A, Luo LF, Wood EF, Wen FH, Mitchell KE, Houser PR, et al. Evaluation of the North American Land Data Assimilation System over the southern Great Plains during the warm season. Journal of Geophysical Research-Atmospheres. Nov.2003 108
64. Campbell GS. SIMPLE METHOD FOR DETERMINING UNSATURATED CONDUCTIVITY FROM MOISTURE RETENTION DATA. Soil Science. 1974; 117:311–314.
65. Cosgrove BA, Lohmann D, Mitchell KE, Houser PR, Wood EF, Schaake JC, et al. Real-time and retrospective forcing in the North American Land Data Assimilation System (NLDAS) project. Journal of Geophysical Research-Atmospheres. Oct.2003 108
66. Yang W, Tan B, Huang D, Rautiainen M, Shabanov NV, Wang Y, et al. MODIS leaf area index products: from validation to algorithm improvement. Geoscience and Remote Sensing, IEEE Transactions on. 2006; 44:1885–1898.
67. Niu GY, Yang ZL, Mitchell KE, Chen F, Ek MB, Barlage M, et al. The community Noah land surface model with multiparameterization options (Noah-MP): 1. Model description and evaluation with local-scale measurements. Journal of Geophysical Research-Atmospheres. Jun. 2011 116
68. N. R. C. S. U.S. Department of Agriculture. , editor. USDA. State Soil Geographic (STATSG0) Data Base Data use information. State College, PA: Penn State University Earth Systems Science Center; 1994.
69. Hansen MC, Defries RS, Townshend JRG, Sohlberg R. Global land cover classification at 1km spatial resolution using a classification tree approach. International Journal of Remote Sensing. Apr.2000 21:1331–1364.
70. Vereecken H, Weihermüller L, Jonard F, Montzka C. Characterization of Crop Canopies and Water Stress Related Phenomena using Microwave Remote Sensing Methods: A Review. gsvadzone. 2012
71. Wigneron JP, Kerr Y, Waldteufel P, Saleh K, Escorihuela MJ, Richaume P, et al. L-band Microwave Emission of the Biosphere (L-MEB) Model: Description and calibration against experimental data sets over crop fields. Remote Sensing of Environment. 107:639–655. 4/30/2007.
72. Kurum M, Lang RH, O'Neill PE, Joseph AT, Jackson TJ, Cosh MH. A First-Order Radiative Transfer Model for Microwave Radiometry of Forest Canopies at L-Band. Geoscience and Remote Sensing, IEEE Transactions on. 2011; 49:3167–3179.
73. Wigneron JP, Calvet JC, Kerr Y, Chanzy A, Lopes A. Microwave emission of vegetation: sensitivity to leaf characteristics. Geoscience and Remote Sensing, IEEE Transactions on. 1993; 31:716–726.
74. Ferrazzoli P, Guerriero L, Wigneron JP. Simulating L-band emission of forests in view of future satellite applications. Geoscience and Remote Sensing, IEEE Transactions on. 2002; 40:2700–2708.
75. Ferrazzoli P, Wigneron JP, Guerriero L, Chanzy A. Multifrequency emission of wheat: Modeling and applications. Geoscience and Remote Sensing, IEEE Transactions on. 2000; 38:2598–2607.
76. Lin B, Sun W, Min Q, Hu Y. Numerical studies of scattering properties of leaves and leaf moisture influences on the scattering at microwave wavelengths. Geoscience and Remote Sensing, IEEE Transactions on. 2008; 46:353–360.
77. Kurum M, O'Neill PE, Lang RH, Joseph AT, Cosh MH, Jackson TJ. Effective tree scattering and opacity at L-band. Remote Sensing of Environment. 118:1–9. 3/15/2012.
78. M. N. a. Chen, K. Harrison, Ed., personal communication, ed, 2014.

79. Choudhury BJ, Schmugge TJ, Chang A, Newton RW. Effect of surface roughness on the microwave emission from soils. Journal of Geophysical Research: Oceans. 1979; 84:5699–5706.
80. Mo T, Choudhury BJ, Schmugge TJ, Wang JR, Jackson TJ. A model for microwave emission from vegetation-covered fields. Journal of Geophysical Research: Oceans. 1982; 87:11229–11237.
81. Hunt ER Jr, Li L, Yilmaz MT, Jackson TJ. Comparison of vegetation water contents derived from shortwave-infrared and passive-microwave sensors over central Iowa. Remote Sensing of Environment. 115:2376–2383. 9/15/2011.
82. Carlson TN, Ripley DA. On the relation between NDVI, fractional vegetation cover, and leaf area index. Remote Sensing of Environment. 1997; 62:241–252. 12//.
83. Jiang Z, Huete AR, Chen J, Chen Y, Li J, Yan G, et al. Analysis of NDVI and scaled difference vegetation index retrievals of vegetation fraction. Remote Sensing of Environment. 101:366–378. 4/15/2006.
84. Grody NC. Surface identification using satellite microwave radiometers. Geoscience and Remote Sensing, IEEE Transactions on. 1988; 26:850–859.
85. Dong X, Xi B, Kennedy A, Feng Z, Entin JK, Houser PR, et al. Investigation of the 2006 drought and 2007 flood extremes at the Southern Great Plains through an integrative analysis of observations. Journal of Geophysical Research: Atmospheres. 2011; 116:D03204.
86. Burke EJ, Gurney RJ, Simmonds LP, Jackson TJ. Calibrating a soil water and energy budget model with remotely sensed data to obtain quantitative information about the soil. Water Resources Research. Jul.1997 33:1689–1697.
87. Hald A. On the history of maximum likelihood in relation to inverse probability and least squares. Statistical Science. May.1999 14:214–222.
88. Holland, JH. Adaptation in Natural and Artificial Systems. University of Michigan Press. , editor. 1975.
89. Prigent C, Liang P, Tian Y, Aires F, Moncet JL, Boukabara SA. Evaluation of modeled microwave land surface emissivities with satellite-based estimates. Journal of Geophysical Research: Atmospheres. 2015; 120:2706–2718.
90. Holmes RR, Koenig TA, Karstensen KA. Flooding in the United States Midwest, 2008. US Geological Survey professional paper. 2010:1–63.
91. Prigent C, Papa F, Aires F, Rossow WB, Matthews E. Global inundation dynamics inferred from multiple satellite observations, 1993–2000. Journal of Geophysical Research: Atmospheres. 2007; 112:D12107.
92. Hamilton SK, Sippel SJ, Melack JM. Comparison of inundation patterns among major South American floodplains. Journal of Geophysical Research: Atmospheres. 2002; 107:LBA 5- 1-LBA 5–14.
93. Fily M, Royer A, Goïta K, Prigent C. A simple retrieval method for land surface temperature and fraction of water surface determination from satellite microwave brightness temperatures in sub-arctic areas. Remote Sensing of Environment. 85:328–338. 5/30/2003.
94. Temimi M, Leconte R, Brissette F, Chaouch N. Dynamic estimation of free water surface coverage from a basin wetness index of the Mackenzie River basin using SSM/I measurements. Canadian Journal of Remote Sensing. 2007-01/01;2007 33:121–129.
95. Montpetit B, Royer A, Wigneron JP, Chanzy A, Mialon A. Evaluation of multi-frequency bare soil microwave reflectivity models. Remote Sensing of Environment. 162:186–195. 6/1/2015.
96. Escorihuela MJ, Kerr YH, de Rosnay P, Wigneron JP, Calvet JC, Lemaitre F. A Simple Model of the Bare Soil Microwave Emission at L-Band. Geoscience and Remote Sensing, IEEE Transactions on. 2007; 45:1978–1987.
97. Wegmuller U, Matzler C. Rough bare soil reflectivity model. Ieee Transactions on Geoscience and Remote Sensing. May.1999 37:1391–1395.
98. Parrens M, Calvet J-C, de Rosnay P, Decharme B. Benchmarking of L-band soil microwave emission models. Remote Sensing of Environment. 2014; 140:407–419. 1//.
99. Lin B, Minnis P. Temporal Variations of Land Surface Microwave Emissivities over the Atmospheric Radiation Measurement Program Southern Great Plains Site. Journal of Applied Meteorology. 2000; 39:1103–1116. 2000/07/01.

100. Cosh MH, Starks PJ, Guzman JA, Moriasi DN. Upper Washita River Experimental Watersheds: Multiyear Stability of Soil Water Content Profiles. Journal of Environmental Quality. 2014; 43:1328–1333. [PubMed: 25603080]

101. Starks PJ, Fiebrich CA, Grimsley DL, Garbrecht JD, Steiner JL, Guzman JA, et al. Upper Washita River Experimental Watersheds: Meteorologic and Soil Climate Measurement Networks. Journal of Environmental Quality. 2014; 43:1239–1249. [PubMed: 25603072]

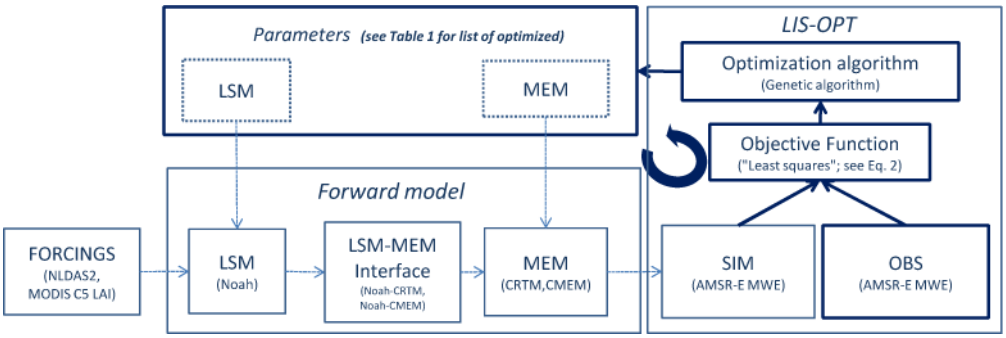

Figure 1.

The overall forward modeling and calibration approach, as implemented within the NASA Goddard Land Information System (LIS)

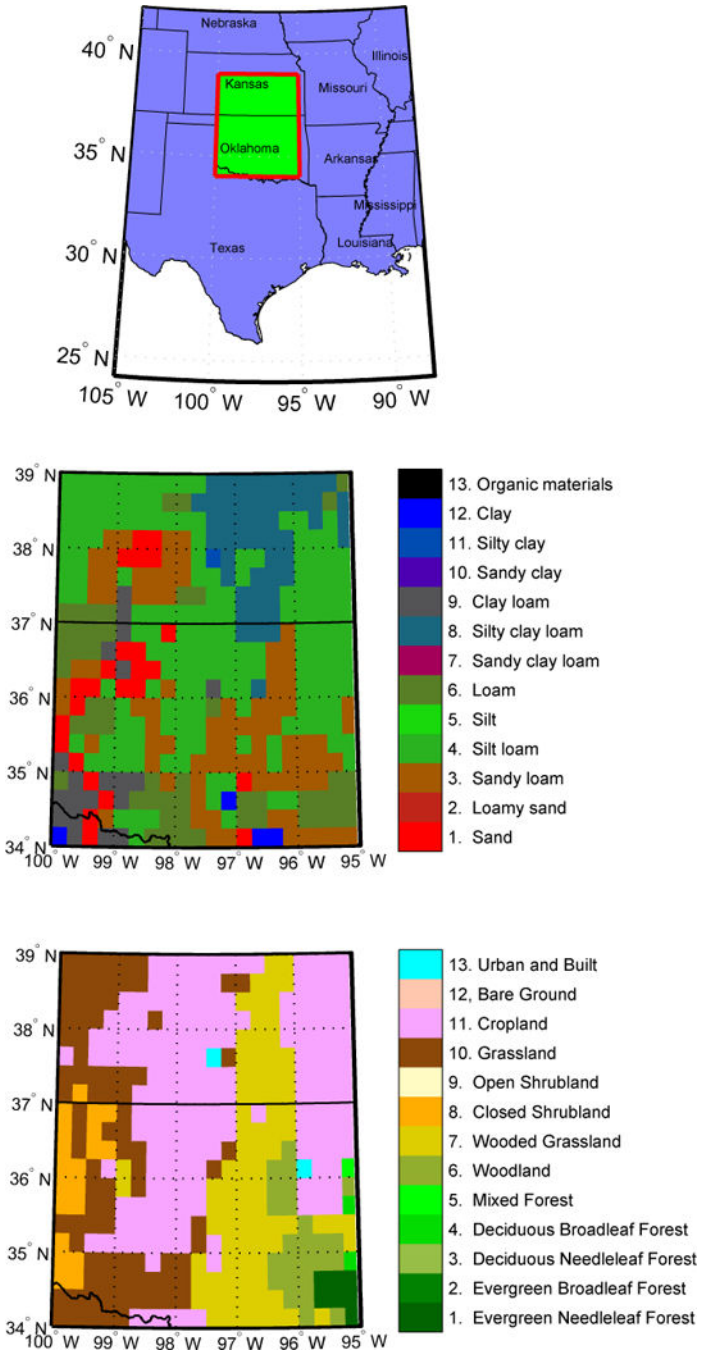

Figure 2.

U.S. Southern Great Plains (SGP) domain (top;[34°N:39°N, 100°W:95°W]), dominant soil texture (middle), and dominant land cover (bottom).

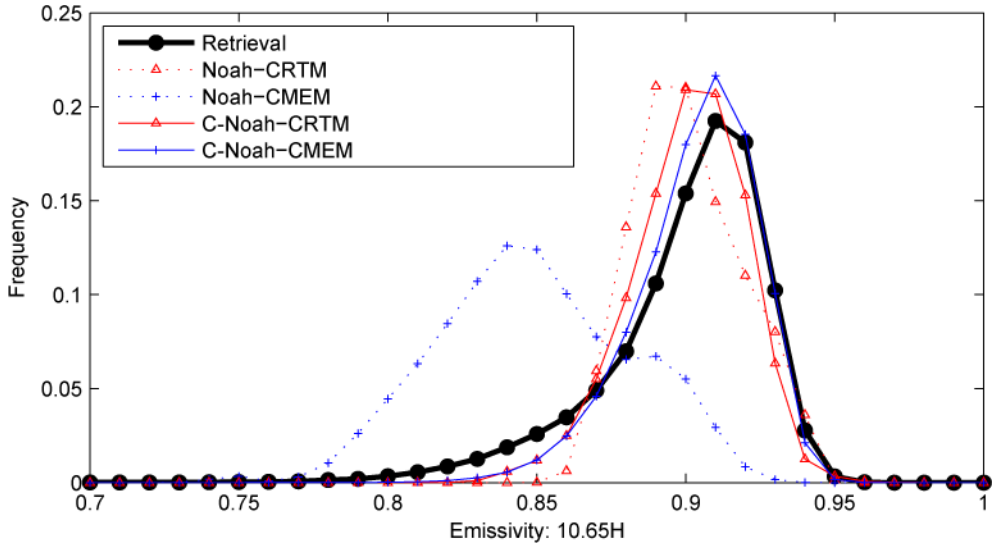

Figure 3.

Estimated probability distribution functions (PDFs) for 10.65 GHz horizontal polarization emissivity across the SGP, for the forward models (un-calibrated and calibrated) and retrievals. As compared to the retrievals, Noah-CMEM has much lower emissivities, while Noah-CRTM has a narrower dynamic range. The calibrated models, C-Noah-CRTM and C-Noah-CMEM, are more in line with the retrievals, but the dynamic range remains too narrow by comparison.

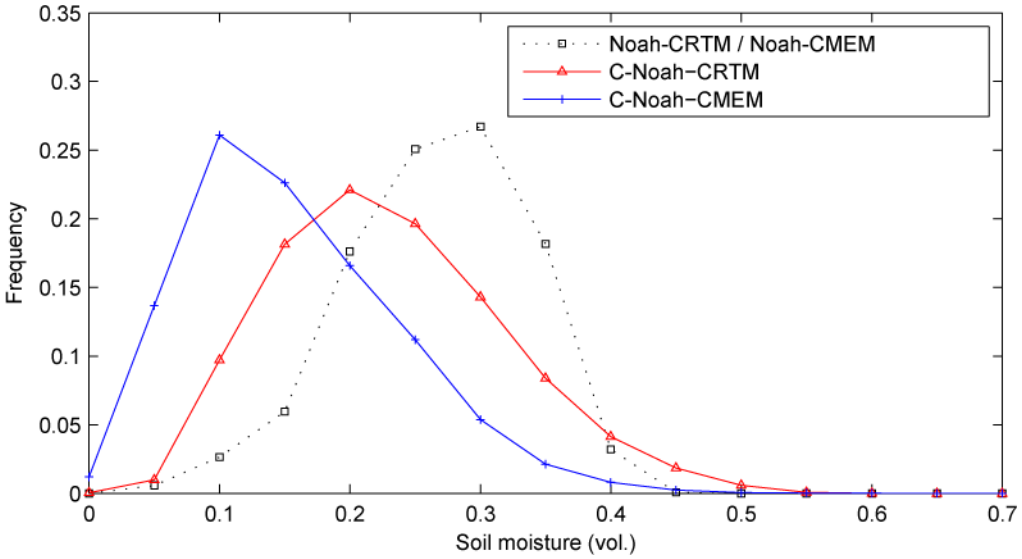

Figure 4.

Estimated probability density functions (PDFs) for soil moisture across the SGP, prior to and after calibration. Calibration to the emissivity retrievals shifts soil moisture to a much drier state, more so for C-Noah-CMEM than C-Noah-CRTM.

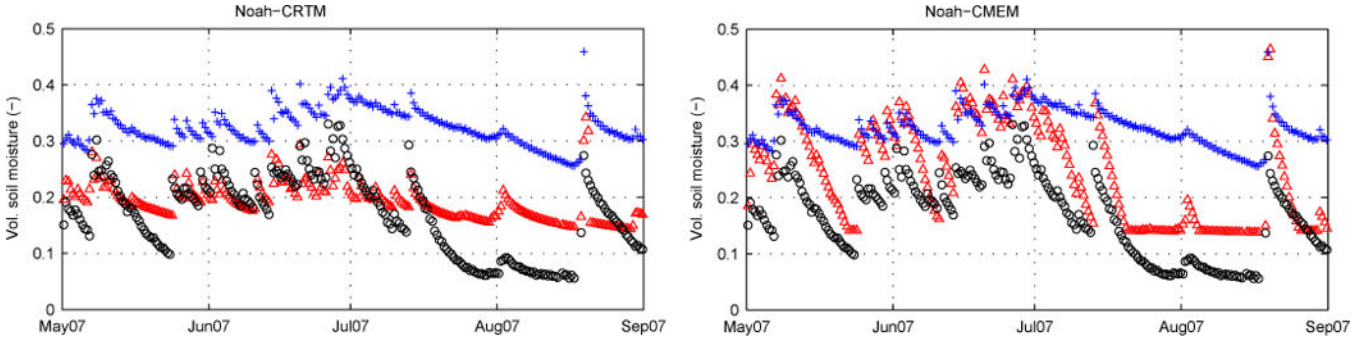

Figure 5.

Overpass-time surface soil moisture time series for uncalibrated Noah (blue plus signs), C-Noah-CRTM (left; red triangles), C-Noah-CMEM (right;red triangles), and USDA ARS Little Washita River Experimental Watershed *in situ* (black circles; 0–5 cm depth)

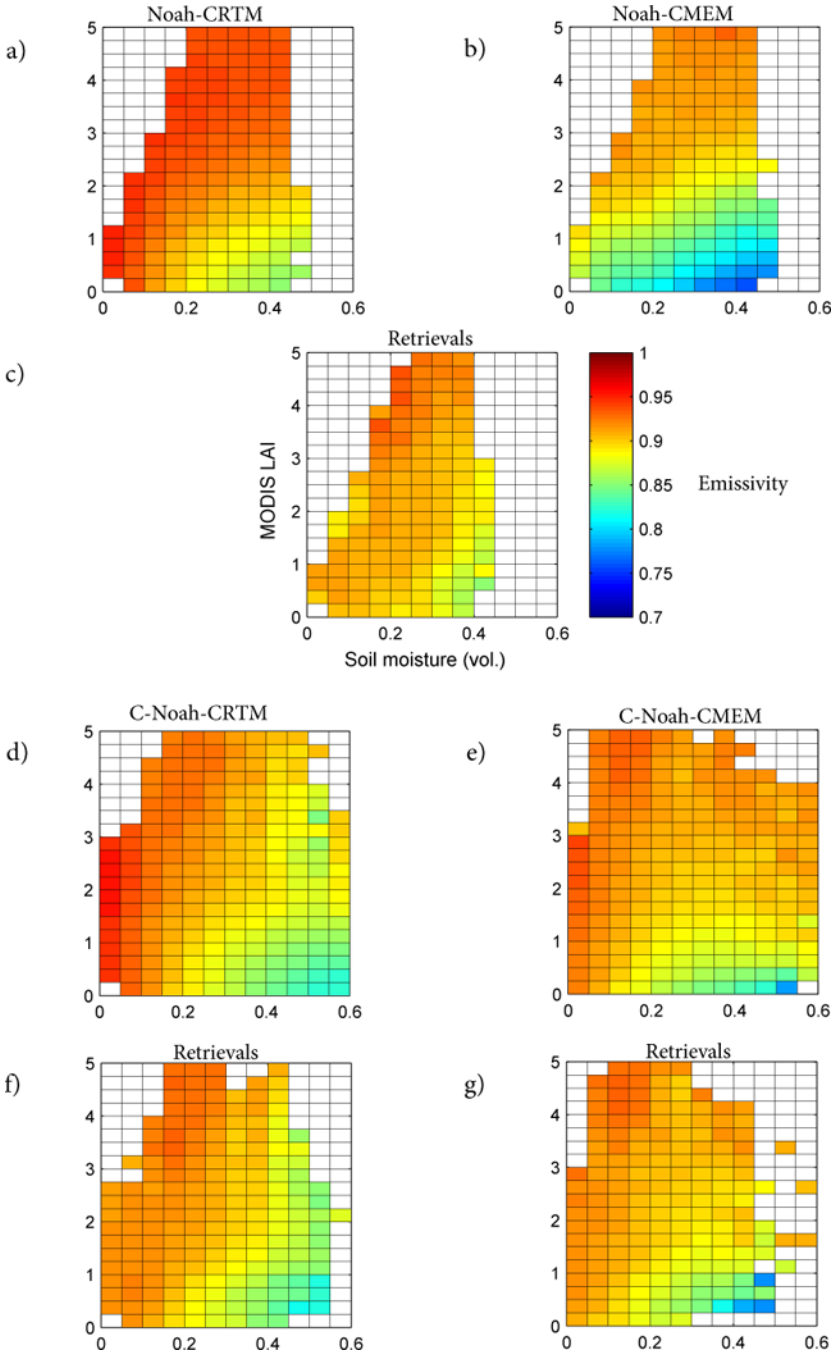

Figure 6.

10.65 GHz horizontal polarization emissivity for bins of soil moisture and LAI, for the models (a,b) and retrievals (c) prior to calibration, and for the models (d,e) and retrievals (f,g) after calibration. Axes are as labeled in c). Soil moisture (x-axis) is as estimated by Noah (a–c), C-Noah-CRTM (d,f), and C-Noah-CMEM (e,g).

Table 1

Forward model parameters subjected to calibration and their allowed ranges.

a) Noah 3.3				
Parameter description	**Model code name**	**Low**	**High**	**Unit**
Maximum volumetric soil moisture (porosity)	SMCMAX	0.1	0.6	m^3/m^3
Saturated soil matric potential	PSISAT	0.01	3.2	
Saturated soil hydraulic conductivity	DKSAT	5.00E-07	3.00E-05	m/s
Saturated soil water diffusivity	DWSAT	6.00E-07	2.40E-05	
“b” parameter in hydraulic functions	BEXP	2.75	12	
Quartz content, used to compute soil thermal diffusivity	QUARTZ	0.02	0.95	
Minimum stomatal resistance	RSMIN	40	1000	s/m
Canopy resistance: radiation stress parameter	RGL	30	150	
Canopy resistance: vapor pressure deficit coefficient	HS	36	55	
Roughness length	Z0	0.01	0.99	m
Leaf area index (set to 4.0 across vegetation classes)	LAI	0.05	6.5	
Canopy water evaporation exponent	CFACTR	0.1	2	
Maximum canopy water capacity	CMCMAX	1.00E-04	2.00E-03	m
Vegetation canopy effect on groundheat flux as function of greenness	SBETA	−4	−1	
Maximum stomatal resistance	RSMAX	2000	10000	
Optimum air temperature for transpiration	TOPT	293	303	K
Parameter used with REFKDT to compute surface runoff parameter KDT	REFDK	5.00E-07	3.00E-05	
Bare soil evaporation exponent	FXEXP	0.2	4	
Surface runoff parameter	REFKDT	0.1	10	
Zilintikevich parameter (controls aerodynamic resistance of atm. surface layer)	CZIL	0.05	0.8	
Soil heat capacity	CSOIL	1.26E+06	3.50E+06	$J/m^3/K$
Ice content threshold above which frozen soil is impermeable	FRZK	0.1	0.25	
Water-equivalent snowdepth upper threshold for 100% snow cover/Max albedo	SNUP	0.01	0.1	m
Soil moisture threshold for onset of some transpiration stress	SMCREF	0	0.5	m^3/m^3
Top layer soil moisture threshold at which direct evaporation from soil ceases	SMCDRY	0	0.15	m^3/m^3
Soil moisture wilting point at which transpiration ceases	SMCWLT	0	0.15	m^3/m^3
Soil thermal diffusivity/conductivity coefficient	F1	−11	0.17	
Deepest soil layer drainage coefficient modifier for slope	SLOPE	0	1	
Surface emissivity	EMISS	0.8	1	–

b) CMEM				
Parameter description	**Model code name**	**Low**	**High**	**Units**
Surface roughness height	SR	0.0002	0.02	m
Leaf thickness	D_LEAF	0.035	0.28	mm
Vegetation water content per LAI	VWC2LAI	0.05	0.7	–
Dry mass fraction of vegetation	M_D	0.1	0.5	–

c) CRTM				
Parameter description	**Model code name**	**Low**	**High**	**Units**
Surface roughness height	SIGMA	0.2	20	mm
Leaf thickness	LEAF_THICK	0.035	0.28	mm
Vegetation water content per LAI	WATER_CONTENT_PER_LAI	0.05	0.3	
Single scattering albedo factor	SSALB_FACTOR	0.85	1.1	

d) Additional tuning parameters				
Parameter description	**Model code name**	**Low**	**High**	**Units**
Fixed bare ground fraction	BGF_FIXED	0	0.4	–
LAI to vegetation greenness fraction factor	K_LAI2VGF	0.2	2	–

Table 2

RMSD of the forward models before and after calibration using AMSR-E retrievals as the benchmark, over the validation period, for the SGP. Calibration greatly improves the consistency with the retrievals but cannot improve upon climatology.

RMSD*100	**10.65V**	**10.65H**	**18.7 V**	**18.7 H**	**36.5 V**	**36.5 H**	**89.0 V**	**89.0 H**	***Ave.***	***Ave. exc. 89***
Noah-CRTM	1.56	2.65	1.81	2.50	1.85	2.48	3.11	3.44	***2.43***	***2.14***
Noah-CMEM	5.56	6.02	4.94	5.59	2.06	2.74	3.01	3.50	***4.18***	***4.48***
C-Noah-CRTM	1.21	2.02	1.51	2.02	1.75	2.02	3.49	3.62	***2.21***	***1.76***
C-Noah-CMEM	1.50	1.86	1.30	1.77	2.59	3.65	4.87	5.98	***2.94***	***2.11***
Climatology	***1.15***	***2.17***	***1.11***	***1.78***	***1.07***	***1.51***	***2.03***	***2.22***	***1.63***	***1.46***

Table 3

Same as Table 2, but after bias correction. After bias correction, the calibrated forward models improve upon climatology by an average of 19% (25% if excluding 89 GHz).

RMSD*100	**10.65V**	**10.65H**	**18.7 V**	**18.7 H**	**36.5 V**	**36.5 H**	**89.0 V**	**89.0 H**	***Ave.***	***Ave. exc. 89***
Noah-CRTM	0.94	1.73	0.95	1.46	0.96	1.28	1.88	2.00	***1.40***	***1.22***
Noah-CMEM	1.00	1.80	0.99	1.45	0.99	1.32	1.80	1.98	***1.42***	***1.26***
C-Noah-CRTM	0.89	1.56	0.92	1.34	0.95	1.21	1.95	2.07	***1.36***	***1.15***
C-Noah-CMEM	0.87	1.43	0.91	1.24	0.95	1.19	1.91	2.02	***1.32***	***1.10***
Climatology	***1.15***	***2.17***	***1.11***	***1.78***	***1.07***	***1.51***	***2.03***	***2.22***	***1.63***	***1.46***

Table 4

RMSD by land cover class for the calibrated forward models (after bias correction). For all classes, use of the calibrated forward models in place of climatology reduces RMSD. The results are very similar for C-Noah-CRTM and C-Noah-CMEM. The greatest percent reduction in RMSE as compared against climatology is for *Cropland*, the predominant land cover class in the SGP, a greater than 20% reduction.

	Average				Average, exc uding 89 GHz			
	RMSD*100		Change from climatology		RMSD*100		Change from climatology	
Land cover	**C-Noah-CRTM**	**C-Noah-CMEM**	**C-Noah-CRTM**	**C-Noah-CMEM**	**C-Noah-CRTM**	**C-Noah-CMEM**	**C-Noah-CRTM**	**C-Noah-CMEM**
1. Evergreen Needleleaf Forest	1.02	1.01	−3	−3	0.72	0.71	−3	−4
4. Deciduous Broadleaf Forest	1.03	1.01	−6	−8	0.72	0.73	−7	−5
5. Mixed Forest	1.09	1.05	−4	−8	0.78	0.78	−6	−6
6. Woodland	1.20	1.19	−7	−8	0.91	0.91	−8	−9
7. Wooded Grassland	1.26	1.20	−11	−15	0.99	0.93	−16	−21
8. Closed Shrubland	1.34	1.29	−13	−16	1.15	1.09	−17	−22
10. Grassland	1.40	1.36	−18	−20	1.23	1.18	−22	−25
11. Cropland	1.44	1.39	−20	−23	1.24	1.19	−26	−29
13. Urban and Built	1.22	1.19	−8	−10	1.11	1.06	−8	−12

Table 5

Change in RMSD, as a percent, if not jointly calibrating the land surface model (LSM) and microwave emissivity model (MEM). In average terms, RMSD is worsened by 1–6%, 2–12% if excluding 89 GHz. The impact is greatest at lower frequencies and if calibrating only the MEM, as high as 23%.

% change in RMSD		10.65V	10.65H	18.7 V	18.7 H	36.5 V	36.5 H	89.0 V	89.0 H	*Ave.*	*Ave. exc. 89*
Noah-CRTM	LSM-only	2.0	2.8	1.9	2.8	0.9	1.5	−0.2	0.0	***1.3***	***2.1***
	MEM-only	5.2	10	2.1	7.2	0.2	3.7	−3.4	−2.5	***2.3***	***5.4***
Noah-CMEM	LSM-only	2.3	5.3	1.1	3.1	1.4	2.8	1.3	2.2	***2.5***	***2.9***
	MEM-only	13	23	5.8	15	2.3	7.8	−5.9	−4.2	***5.6***	***12***